Neutralization of highly charged ions at grazing incidence on a metal surface

P. A. Zeijlmans van Emmichoven
Oak Ridge National Laboratory, Oak Ridge, Tennessee 37831-6372
and Joint Institute for Heavy Ion Research, Holifield Heavy Ion Research Facility, Oak Ridge, Tennessee 37831-6374

C. C. Havener and F. W. Meyer
Oak Ridge National Laboratory, Oak Ridge, Tennessee 37831-6372
(Received 24 September 1990)

Electron energy spectra and total electron yields are studied to provide information on the neutralization of 24-keV N^{q+} ions ($q=2,4,6$) incident at grazing angles on a Cu(100) surface. A computer simulation of the neutralization is presented that assumes resonant neutralization of the ions leading to highly excited "hollow" atoms. Deexcitation of these atoms is assumed to take place by purely intra-atomic Auger transitions. The results of this simulation are not in agreement with our experimental observations. A modified simulation, assuming again resonant neutralization of the ions followed by faster deexcitation processes, and, in addition, fast Auger deexcitation directly into the L shell, shows a much better agreement with the experimental observations.

I. INTRODUCTION

Almost 40 years ago Hagstrum studied electron spectra for collisions between ions and metals surfaces.[1] By using low-energy singly charged ions, he found that electron emission is mainly due to potential emission or, more specifically, due to inter-atomic Auger transitions in which two metal electrons from the valence band are involved. From the energy distribution of the emitted electrons, Hagstrum was able to deduce information on the surface density of states of the metal.

Increasing the charge state of the incident ions results in more complicated electron spectra. For doubly charged ions, evidence was found for interatomic Auger transitions, in addition to resonant transitions from the valence band to the ions followed by intra-atomic Auger transitions.[2,3] For the past few years electron spectra resulting from multicharged ion-surface scattering have been studied. When ions are used that carry an atomic core hole into the collision with the surface, atomic Auger transitions filling these atomic core holes are observed.[4,5] Also target Auger transitions are observed,[4,6] which result from transfer of the projectile vacancies to target atoms. Both projectile and target Auger intensities can serve as excellent probes for the time scale of the neutralization process.[7] However, except for the above-described Auger mechanisms, there is still uncertainty about the neutralization mechanism of multicharged ions at metal surfaces. One neutralization model frequently used in the past is the atomic ladder picture first introduced by Arifov *et al.*[8] In this model, it is assumed that at a certain distance of the ion above the surface resonant transitions occur, transferring electrons from the valence band of the metal to highly excited levels of the ion. These resonant processes are followed by the deexcitation of the atom by means of intra-atomic Auger transitions that lead to the emission of low-energy electrons. Eventually this atomic ladder model results in the filling of the atomic core holes as observed experimentally. However, the time the ions spend in the vicinity of the surface is finite, and therefore the question arises whether this time is sufficient to fill the core holes by this cascade of Auger transitions.

To shed some light on this time problem, we performed a set of measurements on a relatively simple multicharged ion-metal system, namely, N^{q+} ($q=2,4,6$) on Cu(100). Preliminary measurements for the N^{q+} Cu(110) system have been previously reported.[6] The present measurements include electron spectra as well as total electron yields. To vary the time the ions spend above the surface, the measurements were taken as a function of the angle of incidence for a constant incident ion energy of 24 keV. In order to study the neutralization mechanisms, potential emission has to be separated from kinetic emission. This can be accomplished by using the measured spectra in conjunction with the total electron yield measurements and by assuming that kinetic emission is independent of the charge state.[9] To study the neutralization processes within the framework of the atomic ladder picture, a computer simulation was performed that calculates the cascade through the ladder assuming purely atomic Auger rates. Comparison of the measurements with the calculations shows the inability of the atomic ladder model to account for the observed results, providing evidence for additional processes. In the following sections, first some possible neutralization mechanisms will be described, followed by a description of the experimental setup, the measurements, and the computer simulations.

II. NEUTRALIZATION MECHANISMS

A positive ion approaching a metal surface induces a negative image charge at the surface. Classically, the interaction energy between the ion and its image charge is described by $q^2/4z$ (where q represents the charge of the ion and z represents the ion-surface distance). This expression holds for distances down to a few atomic units.[10] The interaction results in an upward shift of the ionic energy levels. If one of these shifted, unfilled levels of the ion has the same energy as the valence band of the metal surface, resonant transitions of electrons from the metal to the ion can occur [Fig. 1(a)]. As depicted in Fig. 1(a),

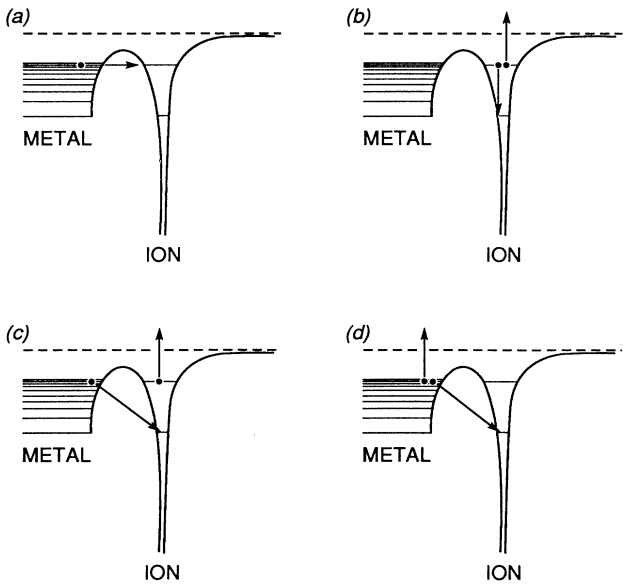

FIG. 1. Energy diagrams describing (a) resonant neutralization, (b) an intra-atomic Auger transition, (c) Auger deexcitation, and (d) an interatomic Auger transition.

the electrons "tunnel" through the potential barrier between the metal surface and the ion. This potential barrier decreases with decreasing ion-surface distance, eventually leading to the possibility of classical overbarrier transitions at a distance of roughly $2q+7$ a.u.[11] These resonant transitions between the metal valence band and the ion lead to multiexcited "hollow" atoms. In the atomic ladder picture, intra-atomic Auger transitions [Fig. 1(b)] lead to a stepwise deexcitation of the atom, and to the emission of low-energy electrons with energies up to about 30 eV.[8] In addition to this "atomic" cascade, there are other mechanisms that can lead to the deexcitation of the multiexcited atom, such as, e.g., Auger deexcitation [Fig. 1(c)]. In an Auger deexcitation process a metal electron is captured by the ion, thereby emitting one of the excited atomic electrons (the roles of the two electrons can be interchanged). The rate for this mechanism will depend strongly on the ion-surface distance because of the involvement of a metal electron.

In addition to the resonant transitions followed by the deexcitation steps, interatomic Auger transitions are also possible, as Hagstrum found for singly charged ions. In such Auger processes two metal electrons are involved. One is captured by the ion, releasing the energy for the other one to be emitted [Fig. 1(d)]. At large distances, the rates for these Auger transitions into the localized core holes are expected to be small compared to the resonant transitions into higher-energy levels.[5] However, the possibility of interatomic Auger transitions into higher-energy levels leading to the emission of low-energy electrons can certainly not be excluded in the overall neutralization of the ions.

The relative contributions of the various neutralization mechanisms are determined by the specific rates. From our measurements we will try to deduce information on which contributions are more important than others.

III. EXPERIMENT

Highly charged nitrogen ions were extracted from the Oak Ridge National Laboratory electron cyclotron resonance (ORNL-ECR) source.[12] Before entering the ultrahigh-vacuum chamber housing the surface experiment, the ions were collimated[6] to a well-defined beam with a maximum angular spread of 0.5°. A Cu(100) crystal was mounted on a manipulator which allowed for two rotations: A 90° azimuthal rotation Φ around the crystal normal and a 360° polar rotation Ψ around the axis perpendicular to the scattering plane (plane containing the beam and the crystal normal). With this setup any orientation of the crystal with respect to the beam could be obtained. A schematic view of the setup is shown as an inset in Figs. 2, 3, and 4. For the experiments described here, the ions were directed along the [001] direction. The electrons emitted in a selected direction were focused on a hemispherical analyzer by a three-element zoom lens (acceptance angle about 3°). After energy selection by the analyzer, the electrons were detected by a channel plate biased at +300 V. The energy resolution of the analyzer was roughly 3% of the transmitted electron energy. The analyzer could be moved in the scattering plane over about 120°. For the measurements described here, the analyzer was preset at an angle of 130° with respect to the incident beam direction. All the spectra that will be shown have been corrected by $1/E$ (E represents the energy of the transmitted electrons) for the energy-dependent transmission of the analyzer.

To obtain the total electron yield γ, the current to the crystal was measured both with and without a positive bias voltage applied to hold the secondary electrons. The total electron yield, defined as the average number of emitted electrons per incoming ion, is given by

$$\gamma=\frac{I_c-I_c^b}{I_c^b/q} \tag{1}$$

where I_c represents the unbiased crystal current at a certain angle of incidence, I_c^b is the biased (+300 V) crystal current for $\Psi=90°$, and q represents the charge state of the incoming ions.

The target bias potential of +300 V leads to at least 95% suppression of all secondary electrons.

IV. MEASUREMENTS

We have performed measurements of the total electron yield and electron energy spectra for 24-keV N^{2+}, N^{4+},

and N^{6+} ions incident on Cu(100). This set of measurements for the different charge states enables us to make a distinction between the contributions due to kinetic and potential emission. The results will be shown below. To study the influence of the neutralization time of the ions on the yields and on the electron spectra, the measurements were taken for different angles of incidence of the ion beam on the crystal.

A. Total electron yields

The variation of the total electron yield with the angle of incidence is shown in Fig. 2. The yields are deduced from the biased and unbiased crystal currents by applying Eq. (1) as described in the preceding section. Also shown in Fig. 2 is the contribution of kinetic emission to the yields. This contribution is estimated from the two lower charge states in the following way. For the lower charge states the dependence of the yields on the total neutralization energy (i.e., the sum of the binding energies of the missing ionic electrons) has been found to be linear.[5,13,14] Assuming kinetic emission to be independent of the charge state of the incoming ions, extrapolation of the yields for N^{4+} and N^{2+} to the yield for a neutral atom gives us an estimate for the contribution of kinetic emission (see, e.g., Ref. 13). An increase of the angle of incidence results in a decrease of kinetic emission as was also found for other measurements using ions at higher incident energies.[15] For these measurements this decrease of kinetic emission has been ascribed to a decrease of the time the ions spend in a region of the solid from which the electrons can escape.

We define the differences between the total electron yields and the kinetic-emission contribution shown in Fig. 2 to be equal to the potential-emission contribution. The dependence of these estimates for potential emission on the angle of incidence is very small. These observations will be discussed in more detail in the next section in combination with the model calculations.

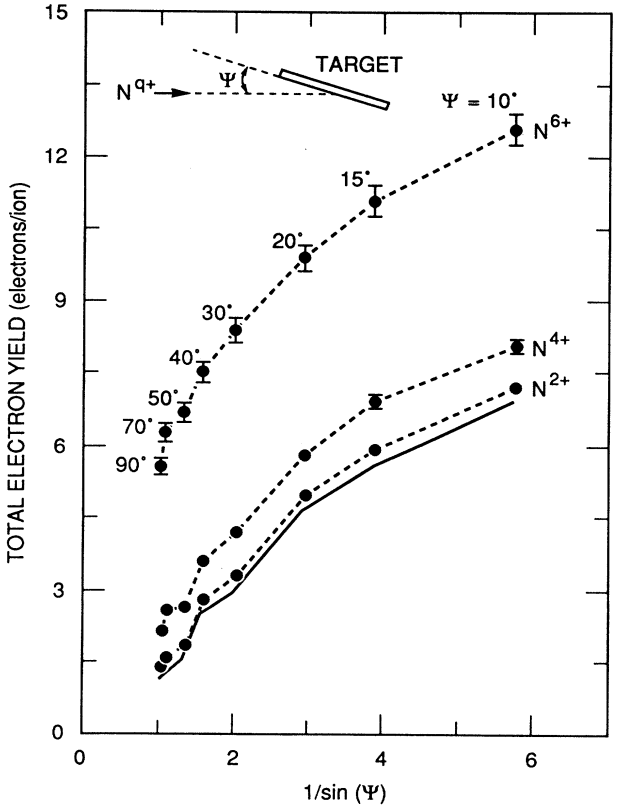

FIG. 2. Measured total electron yields for three charge states of N as a function of the angle of incidence. The error bars not shown are smaller than the size of the data points. Also indicated (solid curve) is the kinetic-emission contribution to the total electron yields as deduced from the N^{4+} and the N^{2+} measurements as explained in the text. A schematic view of the experimental setup is shown in the inset.

B. Electron spectra

The electron spectra obtained for the three different charge states and for angles of incidence of 10° and 20° are shown in Figs. 3 and 4, respectively. The absolute intensity of each spectrum was obtained by normalizing to the corresponding total electron yields (shown in Fig. 2). The total electron intensity contained in a spectrum is equal to the sum of potential emission and kinetic emission at that observation angle. The main part of potential emission is expected to be isotropic. The contribution of potential emission to the spectrum was therefore taken to be equal to the "potential-emission" electron yield (per ion and per steradian). Kinetic emission, on the other hand, has a $\cos\theta$ distribution[16] (with θ the angle with the crystal normal) and therefore the "kinetic-emission" electron yield first had to be corrected for this angular dependence. This normalization was consistent with one based on a calculation of the overall spectrometer efficiency,[7]

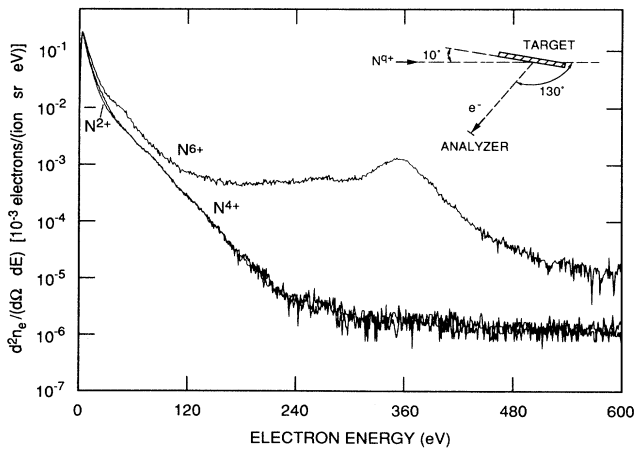

FIG. 3. Normalized electron energy distributions for 24-keV N^{q+} ions incident on Cu(100) at 10° (for three charge states). The experimental situation is shown in the inset.

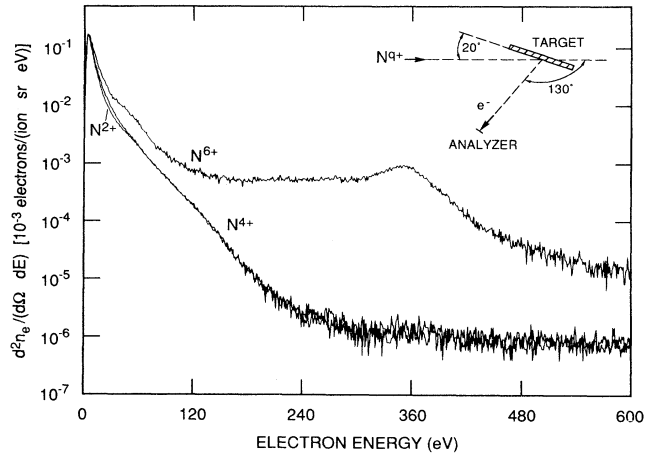

FIG. 4. Normalized electron energy distributions for 24-keV N^{q+} ions incident on Cu(100) at 20° (for the three charge states). The experimental situation is shown in the inset.

using reasonable estimates for the relevant physical parameters.

Both N^{2+} spectra consist mainly of kinetically emitted electrons (more than 95%) as follows directly from Fig. 2. The only discernable structure not due to kinetic emission is the small peak around 260 eV. This structure is ascribed to *KVV* Auger transitions of carbon, present as a contaminant on the surface. The *K*-shell vacancies of carbon are produced in a transfer process via rotational coupling from $2p$ vacancies of the nitrogen projectiles.[6,17,18]

Increasing the charge state of nitrogen from 2+ to 4+ increases the contribution of potential emission to the total electron yields to roughly 15%. Besides the carbon structure around 260 eV an additional structure is observed at low energies (<40 eV). The origin of these low-energy electrons will be discussed later. Evidence for projectile inner-shell excitation as found for 60-keV ions[6] is not found for the present energy of 24 keV (see Figs. 3 and 4).

For N^{6+} the electron emission consists of about 50% potential emission and 50% kinetic emission. Again the carbon *KVV* structure is visible around 260 eV. Comparison of the N^{6+} spectra to the N^{2+} spectra shows that the introduction of a *K*-shell vacancy in nitrogen gives rise to additional electron emission in a broad energy region ranging from about 5 to 500 eV. The feature around 360 eV is due to projectile *KLL* Auger transitions as described in previous work for nitrogen on Au and Cu.[4,6,18] The origin of the additional intensity of the N^{6+} spectrum is best studied after subtraction of the kinetic-emission part of the spectrum.

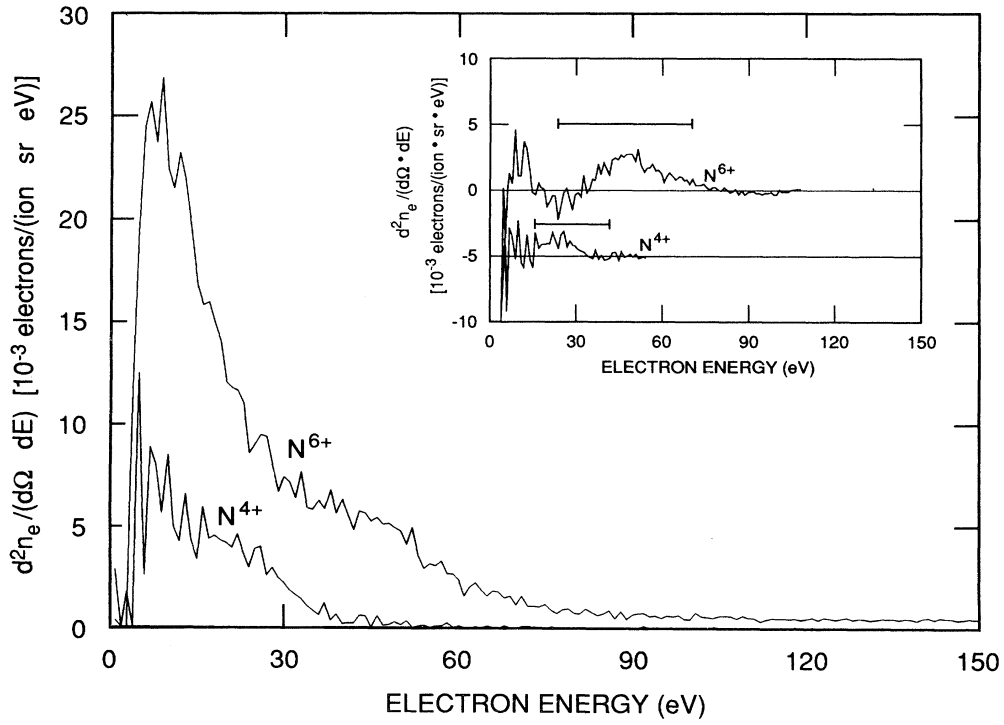

FIG. 5. The low-energy part of the potential-emission spectra for N^{6+} and N^{4+} for 10° angle of incidence. The discrete features are shown separately in the inset in which the underlying background has been subtracted. Also shown in the inset are the calculated *LMM* energy regions.

As was shown in the preceding section, electron emission for N^{2+} at grazing incidence is mainly due to kinetic emission. Therefore we will use this spectrum as an estimate of the kinetic part of the 4+ and 6+ spectra (assuming again that kinetic emission is independent of the charge state of the incoming projectiles.[9,13]). After subtraction of the normalized 2+ spectrum from the normalized higher charge state spectra, the potential-emission contribution remains. The low-energy parts of these difference spectra are shown in Fig. 5 for an angle of incidence of 10°. The results for 20° are comparable. Note that the low-energy part of the potentially emitted electron energy distributions consists of two contributions: A large background intensity peaked at about 10 eV with a tail towards higher energies, and a discrete feature superimposed on this background. The large intensity is possibly due to the small deexcitation and neutralization steps in the higher-energy levels. As described in the second section, various Auger mechanisms can give rise to such small deexcitation steps. The discrete feature is shown separately as an inset in the figure after subtraction of the background. Studying the energy of this discrete peak as a function of the observation angle shows a Doppler shift that is consistent with emission from the moving projectile system. Calculated *LMM* Auger electron energy ranges, obtained using Cowan's Hartree-Fock codes,[19] are also shown in the inset of Fig. 5. The ranges shown include emission from all possible charge states. The agreement between the measured and the calculated, Doppler shifted, energy ranges for *LMM* emission suggests that this structure is due to *LMM* Auger electron emission from the projectile. This conclusion was confirmed by 17-keV O^{7+} measurements grazingly incident on Cu(100), which show a similar discrete feature at slightly higher energies in accordance with the higher Z of oxygen. A similar conclusion was reached by Folkerts and Morgenstern,[20] who used lower-energy hydrogenlike N and O ions incident on polycrystalline tungsten at an angle of 45°.

The high-energy parts of the difference spectra for N^{6+} at incidence angles of 10° and 20° are shown in Fig. 6. For N^{4+} no additional intensity was observed at the higher energies. The N^{6+} spectra consist of a *KLL* peak and a broad structure that extends to low energies. We will first discuss the origin of the peak structure. Also shown in Fig. 6 are calculated *KLL* Auger energy ranges for different charge states, using Cowan's Hartree-Fock codes,[19] that have been appropriately Doppler shifted to permit comparison with the 130° observation angle. The agreement between the measured and calculated energy ranges suggests that the peak is due to *KLL* emission from projectiles that are predominantly neutral or singly charged, as proposed before for O on Au.[6] This also implies that, upon emission of these electrons, the direction of the ions has not changed significantly with respect to the incident direction (this would result in an incorrect Doppler shift) and that the electrons can escape from the surface region without significant energy losses. Electrons emitted above (from incident ions and from ions reflected by the surface with small scattering angles) or immediately below the surface will fulfill these conditions. An estimate of the depth from which the electrons can be emitted without subsequent significant energy losses is the inelastic mean free path, which is at least on the order of 10 a.u. for 360-eV electrons in metals.[21] The broad distribution underlying the peak, on the other hand, we ascribe to subsurface emission followed by elastic and inelastic scattering of the electrons, to emission from significantly scattered ions, and to backscattering from the surface of above-surface emitted electrons.[6,22] This also explains why the broad distribution extends up to energies equal to the energy of the electrons emitted in the forward direction of the ions (indicated by the arrow in Fig. 6). From now on we will refer to this broad distribution as the broad-*KLL* contribution.

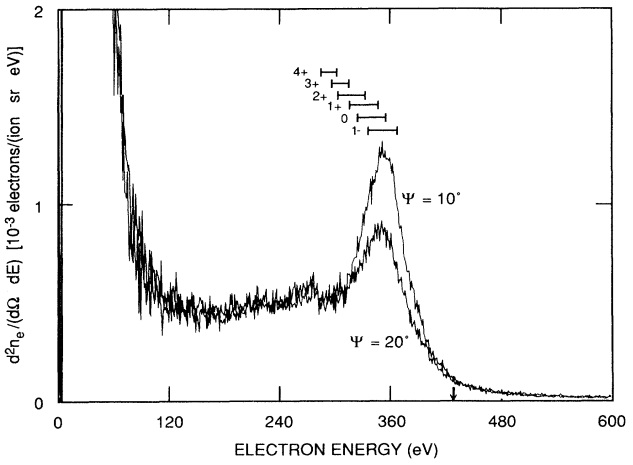

FIG. 6. The high-energy part of the potential emission for N^{6+} for 10° and 20° angles of incidence. Also shown are calculated *KLL* energies for each charge state. The arrow on the horizontal axis denotes the energy of the *KLL* electrons emitted in forward direction.

From the normalized spectra the number of emitted electrons per incoming ion can be deduced for each discernible structure. The numbers for N^{6+}, integrated over 4π, are shown in Table I. Except for the broad-*KLL* contribution for which a $\cos\theta$ distribution was used, all structures were assumed to have an isotropic distribution. For the *LMM* intensity the peak shown in the inset of Fig. 5 was used. To obtain the *KLL* peak intensity, the area of the peak on top of the broad-*KLL* distribution

TABLE I. Number of emitted electrons per incoming ion for N^{6+} incident on Cu(100) for two different angles of incidence. The numbers are derived from the measurements after integration over 4π. Except for the broad-*KLL* contribution, which has been corrected for a cosine emission distribution, isotropic emission was assumed.

	Low-energy component	*LMM*	*KLL*	Broad *KLL*
10°	7.6	0.58	0.44	0.84
20°	7.8	0.36	0.23	0.74

was used. For the broad-*KLL* contribution all the intensity with an energy larger than half the *KLL* energy was taken, but excluding the *KLL* peak itself. This energy region was chosen to avoid "double counting" of electrons induced by the "primary" *KLL* electrons. Because of energy conservation it is impossible for two electrons with an energy larger than half the *KLL* energy to be emitted in one emission event. Integrating this electron energy distribution provides a lower limit for the broad-*KLL* contribution.

According to Table I the *LMM* intensity is slightly larger than the *KLL* peak intensity. This is consistent with the results from Folkerts and Morgenstern.[20] Increasing angle from 10° to 20° increases the perpendicular velocity by roughly a factor of 2, halves the *KLL* intensity, and decreases the *LMM* intensity. The broad-*KLL* contribution and the low-energy component, on the other hand, are only slightly dependent on the perpendicular velocity. Note that for 10° the total *KLL* emission (peak plus broad *KLL*) is larger than 1. This is in part due to double counting of the *KLL* electrons emitted towards the surface (both the *KLL*-emission contributions are integrated over 4π). The numbers summarized in Table I will be used in the next section in combination with the computer simulations.

V. COMPUTER SIMULATIONS AND DISCUSSION

A. The ladder model

We have developed a computer simulation of the deexcitation cascade that results subsequent to the capture of six electrons by a N^{6+} ion. Due to the high charge state of the ion this is a complex problem resulting in many possible electronic configurations. To make the problem tractable, we have made the simplifications described below.

In the simulation a positive ion approaches a metal surface with a constant vertical velocity. At about 20 a.u., resonant neutralization by classical overbarrier transitions becomes possible.[11] However, at larger distances resonant capture of electrons can already occur by quantum-mechanical tunneling. We have therefore chosen a starting distance of 30 a.u., and assumed that six electrons are resonantly captured by the ion into $n=7$. Calculations using Hartree-Fock codes[19] showed that the mean binding energy per electron for the six electrons in $n=7$, after application of the image potential shift, is close to the work function of the metal surface. We assume that these resonant transitions occur instantly. This is justified by the fact that typical resonant neutralization rates for our collision system are on the order of 10^{15} s^{-1}, as follows from a simple calculation using the Fermi velocity and a distance of 30 a.u. above the surface. This rate is fast compared to most deexcitation rates (see Table II).

For this highly excited atom let us first assume that an atomic ladder picture holds, i.e., that intra-atomic Auger transitions occur, leading to the deexcitation of the atom and to the emission of electrons. After the emission of an electron, reneutralization of the ion is assumed to take place by additional resonant electron capture into $n=7$. Deexcitation by intra-atomic Auger transitions can take place via many different channels. In one transition two or more electrons can be involved and various deexcitation energy steps are possible. We allow only for the more probable transitions, i.e., those transitions in which two electrons from the same energy level are involved. Furthermore, only those transitions are taken into account that give rise to the emission of electrons with the lowest possible energy since, in general, the rates decrease significantly with increasing energy of the emitted electrons.[8,23] Atomic states with electrons in $n=6$ and 4 are not included in this ladder because these transitions do not lead to electrons with positive energies.

The above assumptions result in the ladder picture shown in Fig. 7. The neutralization energies of the states shown in this figure were calculated making use of

TABLE II. The intra-atomic Auger rates entering the calculations in 10^{14} s^{-1} as calculated with Cowan's Hartree-Fock codes (Ref. 19). In the rows the rates for the transitions from a certain n level to a lower-lying level are indicated (3-2 means, e.g., from the M shell into the L shell). The population numbers for both levels are denoted in the different columns (4/2, e.g., means four electrons in the upper level and two in the lower one). Exceptions are the *KLL* transitions for which the population numbers of the lower levels are always 1.

	6/0	5/1	4/2	3/3	2/4	5/0	4/1	4/0
2-1	1.7			0.87	0.58			
3-2								11.0
5-3						1.35	0.39	0.97
7-5	1.9	0.60	0.27	0.12	0.030	1.5	0.43	1.08
	3/2	3/1	3/0	2/3	2/2	2/1	2/0	
2-1								
3-2		2.64	6.6		0.55	0.88	2.2	
5-3		0.23	0.58	0.035	0.048	0.077	0.19	
7-5	0.16	0.26	0.65	0.039	0.054	0.086	0.22	

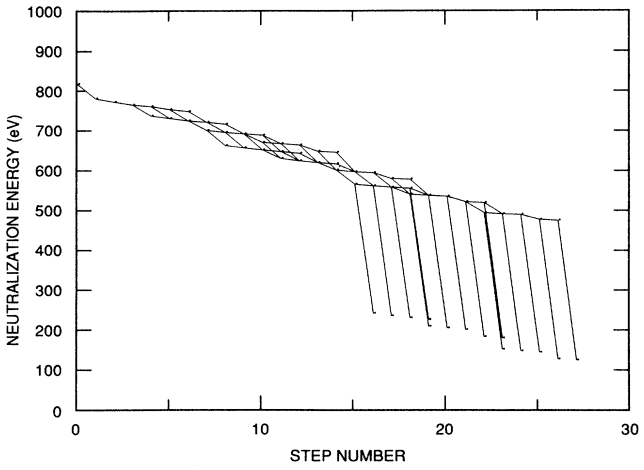

FIG. 7. "The atomic ladder picture." The neutralization energy of the states (denoted by the small dots) used in the calculations as a function of the number of neutralization steps. The transitions between the states are denoted by solid lines.

Cowan's Hartree-Fock codes.[19] The states are denoted by the small dots, the transitions between two states by solid lines. The initial state, with only one electron in the K shell, has a neutralization energy of more than 800 eV. After the simultaneous transfer of six electrons into $n=7$, the second state is reached. After the first intra-atomic Auger transition, a state is reached with one electron in the K shell, one electron in $n=5$, and five electrons in $n=7$. After another intra-atomic Auger transition, a state is reached with one electron in the K shell, two electrons in $n=5$, and four electrons in $n=7$. At this point the ladder branches due to the possibility of an Auger transition from $n=7$ into $n=5$ and from $n=5$ into the M shell. All such small deexcitation steps lead to a gradual decrease of the neutralization energy of the states. After at least 15 steps, states with two electrons in the L shell are populated. KLL transitions now become possible, leading to large changes in the neutralization energy (see Fig. 7).

To calculate the evolution of the population of the states shown in Fig. 7 as a function of the ion-surface distance, a set of coupled differential equations has to be solved. The population of each atomic state n_i is described by its rate equation

$$\frac{dn_i}{dt}=\sum_j(\Gamma_{ji}n_j-\Gamma_{ij}n_i)\leftrightarrow\frac{dn_i}{dz}=\frac{1}{v_v}\sum_j(\Gamma_{ji}n_j-\Gamma_{ij}n_i) \tag{2}$$

where v_v represents the vertical velocity of the ion, z the ion-surface distance, and Γ_{ij} the rate for an atomic Auger transition from state i to state j. The rates were estimated using Cowan's Hartree-Fock codes.[19] The atomic rates that were used are given in Table II.

Solving this set of coupled differential equations for the initial conditions $z=30$, $n_1=1$, and $n_i=0$ for $i\neq1$ gives us the population of all states as a function of the ion-surface distance. The results will be shown in terms of the average number of electrons per ion occupying each of the five relevant principal quantum shells as a function of the distance above the surface. Furthermore, the total number of emitted electrons ("potential-emission" electron yield) as well as the number of emitted electrons in KLL and LMM transitions follow immediately from the calculations. These calculated numbers can be compared to the experimental yields, and to the Auger transition intensities we found experimentally (Table I). The agreement between the measured and calculated peak intensities will be an indication of the validity of the atomic ladder picture. Of course we also have to consider carefully the limitations of the simulation.

As discussed in the preceding section, the experimentally measured KLL peak intensities can also contain contributions from emission just below the surface. This does not influence the comparison between the measurements and the calculations, because for the calculations only the total distance where the resonant transitions and the Auger transitions occur is important. Whether the calculations start at 30 a.u. above the surface and stop at 5 a.u. below the surface makes no difference (except that, in the calculations, we do not take into account subsurface inelastic electron scattering). As until now, we will refer to the distance z used in the calculations as the ion-surface distance. In addition to these subsurface contributions, the measured peak intensities can also contain contributions from reflected ions. The importance of these contributions will be discussed elsewhere.[7]

B. Calculations and Discussions

The results of the calculations using the atomic rates (Table II) for 24-keV ions incident at 10° are shown in Fig. 8. The average number of electrons occupying the principal quantum shells of the N atoms are shown as a function of the ion-surface distance. For clarity the $1s$ electron that is present in the initial ion is omitted. At 30 a.u. the $n=7$ shell is populated by six electrons. As the ion-surface distance decreases the $n=5$ shell is populated by intra-atomic Auger transitions. The population of the M shell just starts in the neighborhood of the surface whereas the K shell and the L shell remain completely unfilled. This is in strong disagreement with our experimental results which show that the K shell was filled for 44% of the ions (see Table I). The calculated "potential-emission" electron yields are also much smaller than the measured ones as shown in Fig. 9 for different vertical velocities. The calculations are represented by the short-dashed line. In calculating the yields shown, it was assumed that all the electrons emitted towards the surface are absorbed. The effects of electron scattering by the surface and secondary electron emission were thus not taken into account here. Also shown in Fig. 9 are some experimental results obtained by Fehringer *et al.*[13] (dot-dashed line), who measured total electron yields for N^{6+} normally incident on polycrystalline tungsten. Obviously, in the present simulation, the deexcitation of the highly excited atom is not fast enough to explain both experimental results. To account for a possible stronger

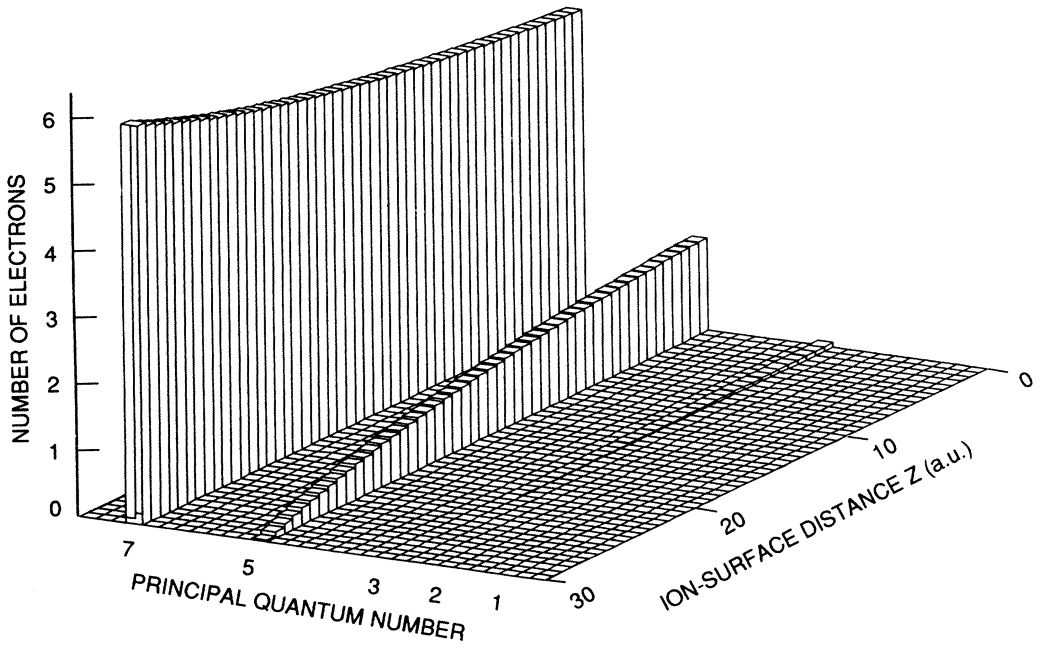

FIG. 8. The calculated distribution of the electrons over the principal quantum shells as a function of the ion-surface distance deduced from the atomic ladder picture. In these simulations the calculated atomic rates were used.

influence of quantum-mechanical tunneling, the calculations were performed again for larger starting distances. However, even increasing the starting distance up to 100 a.u. did not give rise to any *KLL* emission and only to the emission of 0.03 *LMM* electrons per incoming ion. The calculated "potential-emission" electron yields were again much too small compared to the measured ones. Another possible explanation for the failure of the simulation is the faster deexcitation of the highly excited atoms due to the—less probable—larger intra-atomic Auger steps (not included in the calculations). However, the calculation using the increased starting distance can also be regarded as equivalent to one in which the overall deexcitation rate has been enhanced by a factor of 3.3. Using Cowan's Hartree-Fock codes,[19] we have calculated that the rates for the Auger transitions from $n=7$ to 3 are roughly a factor of 20 smaller than the rates from $n=7$ to 5 (from $n=7$ to 4 this factor is about 5). Because of the significantly reduced rates, the effect of such larger Auger steps on the overall deexcitation rate will be much smaller than a factor of 3.3. From the above-described calculations we conclude that the atomic ladder picture, using the Hartree-Fock rates, predicts neutralization rates which are far too slow to explain our experimental results.

It is of course possible that the deexcitation of highly excited atoms close to metal surfaces may take place much faster than estimated by purely intra-atomic Auger rates. This would not be surprising because the atomic character of the Auger transitions between the higher n levels may be questionable when one or more of these levels are degenerate with the valence band of the metal surface. The involvement of metal electrons in the deexcitation processes leading to, for instance, Auger deexcitation or interatomic Auger transitions (see Sec. II) may also cause larger deexcitation rates. In addition to such metal involved mechanisms, an enhancement of the intra-atomic Auger rates due to the interaction between the ion and the metal surface may play a significant role and may also result in a faster deexcitation of the atoms. To simulate such a faster deexcitation, a second calculation was performed still using the atomic rates for the inner-shell transitions, but enhanced atomic rates for the transitions from $n=7$ to 5 and for $n=5$ to the M shell. By multiplying these atomic rates by a factor of 100, a considerable population of the K shell was obtained, in agreement with experiment. The results for this calculation are shown in Fig. 10 and as the long-dashed line in Fig. 9. Already at 30 a.u. the $n=5$ shell and the M shell start to become populated, followed by the population of the L shell and the K shell closer to the surface. However, although the calculated *KLL* emission is now consistent with the measurements, other important inconsistencies remain. For instance, the experimentally derived ratio of *LMM* to *KLL* electrons was slightly larger than 1 (Table I), whereas in the calculations this number turns out to be roughly 7. In addition, increasing the perpendicular velocity by a factor of 2 in the experiments leads to a decrease of the observed *KLL* intensity by a factor of 2 (Table I). The calculations, however, show a much

stronger dependence of the *KLL* intensity on the perpendicular velocity. This is due to the fact that both the population of the *K* shell and the *L* shell are time limited (see Fig. 10). Furthermore, the calculated "potential-emission" electron yields are inconsistent with the measured ones, as shown in Fig. 9. We conclude therefore that by simply increasing the atomic rates for the transitions between the higher-energy levels by a factor of 100, satisfactory agreement between the measurements and calculations cannot be obtained.

So far atomic rates were used for the population of the *L* shell. For large distances this is probably a good assumption, because both the *L* shell and the *M* shell are well below the valence band. However, when the ion-surface distance decreases and the energy levels rise due to the image potential interaction, the rates for mechanisms involving the metal (e.g., Auger deexcitation directly populating the *M* and the *L* shell may possibly become significant. To simulate one possibility, a third calculation with the inclusion of Auger deexcitation directly into the *L* shell was performed. Another possibility, namely the direct population of the *M* shell, will be explored in a separate publication.[7] For this calculation, the rate of filling the *L* shell with six electrons was assumed to be a step function that is 0 at large distances and 10^{15} s^{-1} at small distances. The distance where the step itself occurs was introduced as a parameter into the calculations. We started the calculations again at 30 a.u. To match the calculated *KLL* and the *LMM* yield with the measured values, the atomic rates for the transitions from $n=7$ to 5 and from $n=5$ to the *M* shell were multiplied by a factor of 20 and the distance at which Auger deexcitation into the *L* shell starts was chosen to be 8 a.u. The results of these calculations are shown in Fig. 11. At large distances a ladder-type picture holds which gives rise to *LMM* emission and only very limited *KLL* emission. At a distance of 8 a.u. "loading" of the *L* shell by fast Auger deexcitation starts. This results in a considerable population of the *L* shell and to subsequent emission of *KLL* electrons. For this calculation the dependence of the *KLL* yield on the perpendicular velocity is consistent with the dependence observed experimentally. The dependence of the calculated "potential-emission" electron yield on the perpendicular velocity is shown as the solid line in Fig. 9. The mechanism included in this calculation all give rise to the emission of electrons. The increase of the "potential-emission" electron yield at low energies is caused by the ladder with the enhanced rates for the transitions between the higher-energy levels. The fact that the curve levels off towards higher perpendicular velocities is due to the fast Auger deexcitation processes into the *L* shell at small distances. The agreement between the measured and the calculated yields is much better than for the previous calculations. This agreement also implies that significant contributions of resonant transfer of electrons from the valence band into lower-lying energy levels do not seem very likely. As discussed before, subsurface emission can contribute to the *KLL* peak and, therefore, the reference plane for the distances used in the calculations is not necessarily coincident with the surface. This implies that the loading distance of 8 a.u. can be closer to the surface and can in fact coincide with the surface plane. In the latter extreme, *KLL* emission occurs primarily below the surface.[7] As will be discussed elsewhere, in the event of direct loading of the *M* shell, even the *LMM* emission may occur below the surface.

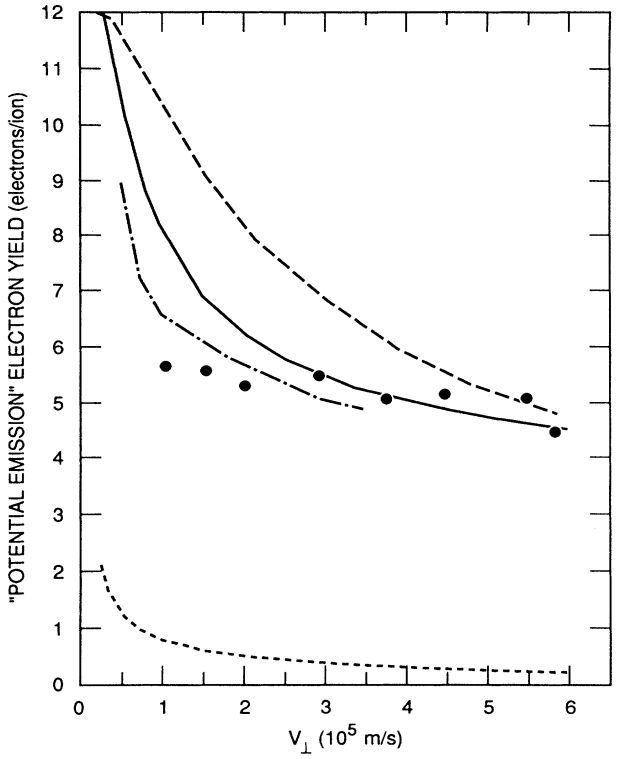

FIG. 9. Measured and calculated "potential-emission" electron yields. The data points indicate our present measurements, the dot-dashed line represents the experimental results from Fehringer *et al.* (Ref. 13). The short-dashed line represents the simulated yields using the intra-atomic Auger rates. The long-dashed line represents the simulated yields with the enhanced atomic rates for the population of the $n=5$ shell and the *M* shell (factor of 100). The solid line represents the simulated yields with the enhanced atomic rates for the transitions between the higher-energy levels (factor of 20) and, in addition, Auger deexcitation directly into the *L* shell starting at a distance of 8 a.u.

VI. CONCLUDING REMARKS

We have performed measurements and computer simulations to shed some light on the complex picture of the neutralization and the deexcitation of a multicharged ion close to a metal surface. In the simulations some assumptions had to be made to approach this complex problem. However, important information on the neutralization and deexcitation mechanisms could be deduced. A simulation, based on the resonant transitions of metal electrons into a high-energy level of the atom followed by the

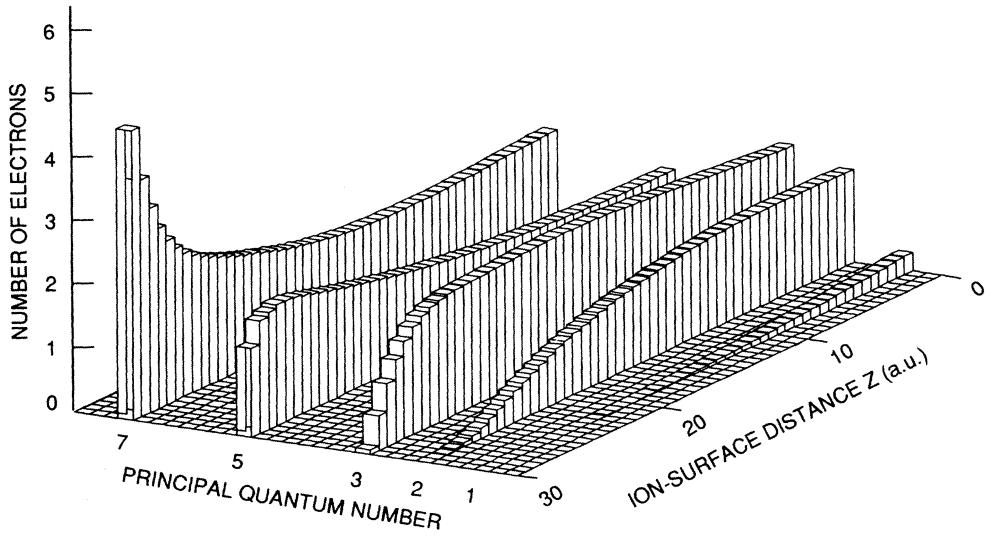

FIG. 10. Same as Fig. 8, but with the atomic Auger rates for the transitions between $n=7$ and 5 and between $n=5$ and the M shell increased by a factor 100.

deexcitation of this highly excited atom by purely atomic Auger transitions, cannot explain our experimental observations. Using enhanced atomic rates for the Auger transitions between the higher-energy levels does not lead to a good agreement between the measurements and the calculations. A much better agreement was obtained using enhanced atomic rates for the Auger transitions between the higher-energy levels, and, in addition, assuming that below a certain distance fast Auger deexcitation directly into the L shell occurs.

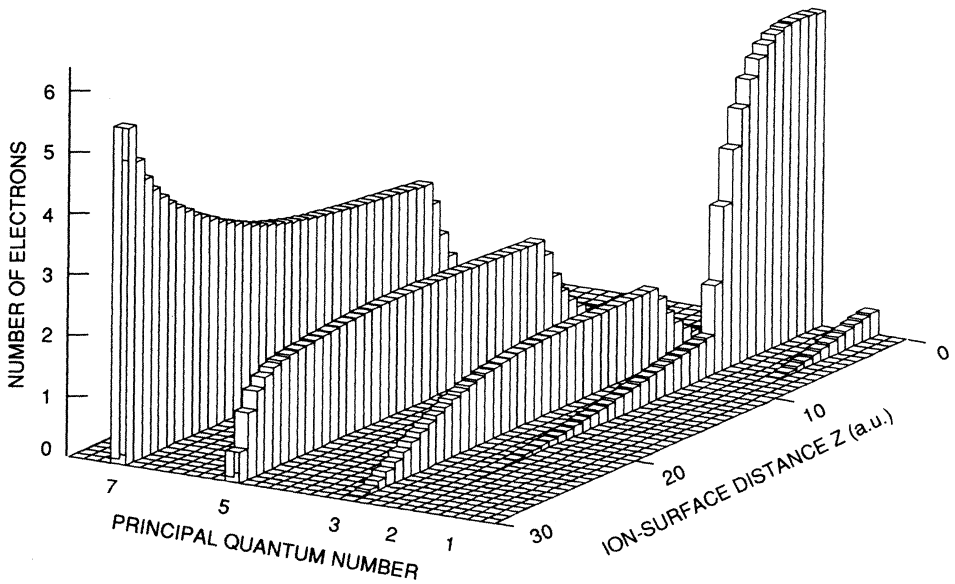

FIG. 11. Same as Fig. 8, but with the rates for the population of the $n=5$ shell and the M shell increased by a factor of 20 and Auger deexcitation directly into the L shell starting at a distance of 8 a.u.

ACKNOWLEDGMENTS

We are indebted to D.M. Zehner for stimulating discussions and for providing us with the essential parts of the apparatus. We would like to thank J. Hale and G. Ownby for their skilled technical assistance. This work was supported by the Office of Basic Energy Sciences, Division of Chemical Sciences, U.S. Department of Energy, under Contract No. DE-AC05-84OR21400 with Martin Marietta Energy Systems, Inc., and the Joint Institute for Heavy Ion Research through Contract No. DE-FG05-87ER40361 with the University of Tennessee.

[1]H. D. Hagstrum, Phys. Rev. **96**, 336 (1954).
[2]H. D. Hagstrum and G. E. Becker, Phys. Rev. B **8**, 107 (1973).
[3]P. A. Zeijlmans van Emmichoven, P. A. A. F. Wouters, and A. Niehaus, Surf. Sci. **195**, 115 (1988).
[4]F. W. Meyer, C. C. Havener, K. J. Snowdon, S. H. Overbury, D. M. Zehner, and W. Heiland, Phys. Rev. A **35**, 3176 (1987).
[5]S. T. de Zwart, Ph.D. thesis, University of Groningen, The Netherlands, 1987.
[6]F. W. Meyer, C. C. Havener, S. H. Overbury, K. J. Reed, K. J. Snowdon, and D. M. Zehner, J. Phys. (Paris) **50**, 263 (1989).
[7]F. W. Meyer, S. H. Overbury, C. C. Havener, P. A. Zeijlmans van Emmichoven, and D. M. Zehner (unpublished).
[8]U. A. Arifov, L. M. Kishinevskii, E. S. Mukhamadiev, and E. S. Parilis, Zh. Tekh. Fiz. **43**, 181 (1973) [Sov. Phys.—Tech. Phys. **18**, 118 (1973)].
[9]M. Delaunay, M. Fehringer, R. Geller, D. Hitz, P. Varga, and H. Winter, Phys. Rev. B **35**, 4232 (1987).
[10]P. M. Echenique, R. H. Ritchie, N. Bárberan, and J. Inkson, Phys. Rev. B **23**, 6486 (1981).
[11]K. J. Snowdon, Nucl. Instrum. Methods Phys. Res. B **34**, 309 (1988).
[12]F. W. Meyer, Nucl. Instrum. Methods Phys. Res. B **9**, 532 (1985).
[13]M. Fehringer, M. Delaunay, R. Geller, P. Varga, and H. Winter, Nucl. Instrum. Methods Phys. Res. B **23**, 245 (1987).
[14]S. T. de Zwart, A. G. Drentje, A. L. Boers, and R. Morgenstern, Surf. Sci. **217**, 298 (1989).
[15]E. J. Sternglass, Phys. Rev. **108**, 1 (1954).
[16]K. H. Krebs, Fortschr. Phys. **16**, 419 (1968).
[17]D. Schneider and N. Stolterfoht, Phys. Rev. A **19**, 55 (1979).
[18]C. C. Havener, K. J. Reed, K. J. Snowdon, D. M. Zehner, and F. W. Meyer, Radiat. Eff. Defects Solids **109**, 99 (1989).
[19]R. D. Cowan, *The Theory of Atomic Structure and Spectra* (University of California Press, Berkeley, 1981).
[20]L. Folkerts and R. Morgenstern, *The Penetration of Charged Particles in Matter,* Proceedings of the 12th Werner Brandt International Conference on the Penetration of Charged Particles in Matter (Oak Ridge National Laboratory, Oak Ridge, TN, 1990), pp. 389–396; Europhys. Lett. **13**, 377 (1990).
[21]B. Lesiak, A. Jablonski, Z. Prussak, and P. Mrozek, Surf. Sci. **223**, 213 (1989).
[22]K. J. Snowdon, C. C. Havener, F. W. Meyer, D. M. Zehner, and W. Heiland, Phys. Rev. A **38**, 2294 (1988).
[23]H. J. Andrae, in *Proceedings of the NATO Summer School on Atomic Physics of Highly Charged Ions,* edited by R. Marrus (Plenum, New York, 1989).